# Finite-Element Modeling of the Global Ocean Tides and Currents in the Time Domain

Kuo, John T.

Veröffentlicht in:
Abhandlungen der Braunschweigischen Wissenschaftlichen Gesellschaft Band 40, 1988, S.101-128


Verlag Erich Goltze KG, Göttingen

# Finite-Element Modeling of the Global Ocean Tides and Currents in the Time Domain

Von **John T. Kuo,** Columbia University in the City of New York

Vorgelegt von Otto K. Rosenbach

(Eingegangen am 14.10.1988)

The problem of numerical modeling of tides and currents in the global oceans over an elastic Earth with realistic continental boundaries and bathymetries that are driven by the tidal generating forces of the Moon and the Sun has ever challenged numerical modelers.

All the numerical models for the global ocean tides have been restricted to the finite difference method and to solving the Laplace's Tide Equations in the frequency domain. Schwiderski, however, was able to improve Zahel's tidal model by tide-gauge observational constraints, and to yield one of the best global tidal models available today.

We have taken an entirely different approach toward the objective of solving the problem of the global ocean tides and currents. We solve solely the vertically integrated hydrodynamic (or so called shallow-water) equations in the time domain without resorting to any tide-gauge observational constraints. We use the semi-implicit finite element method that (1) provides the flexibility in variable element size and shape to adequately discretize highly irregular continental boundaries, particularly around reentrant corners and rapidly varying bathymetries in trenches and continental margins, and (2) achieves numerical stability and convergence for large time steps in the time integration. Moreover, for tidal generating forces, we make use of the precise ephemerides of the Moon and the Sun, instead of using the harmonic development of tidal species.

Finite element results of the global ocean tides so obtained are compared favorably with the SEASAT altimeter data, as a first test, in the Pacific Ocean, and are comparable to the relative precision of Schwiderski's tidal model. They are better than Schwiderski's tidal model in the region where tide-gauge observations are lacking, for instance, in the northeastern Pacific Ocean and Gulf of Alaska.

## Introduction

Since Dietrich published his celebrated cotidal charts of the world oceans for the major diurnal and semi-diurnal tidal constituents in 1944 (Dietrich, 1944), considerable efforts have been directed toward a better understanding of open ocean tides, principally through numerical integration of Laplace's Tide Equations (Tiron et al, 1967; Pekeris and Accad, 1969; Zahel, 1970; Hendershott and Munk, 1970; Parke and Hen-

dershott, 1980; and others). Recently, Schwiderski (1980a, 1980b, 1980c, etc.) incorporated a global distribution of tide-gauge results into the numerical solutions of oceans, i.e. he constrained the Zahel-model by tide-gauge observations principally through varying eddy viscosity.

The assumptions in the formulation of the Laplace's Tide Equations (LTE) have been:

1. a spherical, rigid, and rotating Earth, i.e., neglecting the kinematic ellipticity $m$ and the figure ellipticity $e$, where $e \doteqdot m \sim 3 \times 10^{-3}$ for the actual Earth.
2. a uniform gravitational field, i.e., neglecting the variation of gravitational accelerations $\delta g$ from the pole to the equator, where $\delta g \sim 5 \times 10^{-3}$.
3. a perfect, homogeneous, shallow ocean uniformly covering the rigid Earth, i.e., the parameters $\gamma = gh/c^2$, $s = hN^2/g$, and $\delta = h/a$ are all equal to zero, where $h$ = the average depth of the ocean, $c$ = the sound velocity of water, $N$ = Väisäla frequency, and $a$ = the the mean radius of the Earth, i.e., neglecting $\gamma \sim 2.3 \times 10^{-2}$, $s \sim 1.8 \times 10^{-3}$, and $\delta \sim 7 \times 10^{-4}$ for the actual Earth.
4. a small disturbance relative to a state of uniform rotation, i.e., permitting the linearization of the equations of the motion and neglecting the Coriolis acceleration associated with the horizontal component of the rotation of the Earth and the vertical component of the particle acceleration.

One of the controversies early on has been the neglect of the vertical component of the particle acceleration in the formulation. Bjerknes et al (1933) questioned the validity of the neglect of the vertical component of the particle acceleration so that a class of free inertial oscillation of the homogeneous fluid is excluded. In defense of the validity of LTE for the barotropic motion, Proudman (1942) argued that these free oscillations as major tidal constituents of astronomically forced tide are effectively eliminated except the generations of the $K2$ constituent near the poles and of the long-period constituents at the equator. Miles (1974) reexamined the early controversy more rigorously and concluded that LTE provide a uniformly valid approximation to the barotropic tidal modes for a homogeneous ocean uniformly covering the Earth with relative errors of principally $\gamma$ and $\delta$ of the order as given above for the actual oceans of the Earth.

Concerning the assumption that the Earth is rigid, progress has been made during the last two decades by taking into account the effects of the deformation of the Earth as a result of the astronomical tidal-generating forces on the ocean tide and the interaction of earth and ocean tides. Previous numerical modelers have already made the necessary corrections for these influences in their LTE modeling for the actual oceans (e.g., Pekeris, 1978; Schwiderski, 1980a, b).

However, all the numerical modelers of ocean tides in the past were generally restricted to a single frequency. The reason of traditionally treating the experimental results by harmonic analysis lies in the possibility of reducing the systematic influences of meteorological and other disturbances. These perturbations may well question the validity of a comparison of the theoretical total-tide with the experimental total-tide result without resorting to harmonic analysis.

For many applications, particularly to time-dependent geodesy, satellite orbital perturbations, etc., it is the integrated earth-ocean system, including the tidal and load deformation of the Earth as well as the interaction of the earth and ocean tides that is of interest. By summing up a great number of harmonic terms, it is, in principle, possible to recover the integrated time-varying ocean tides. The most important advantage of treating the ocean tides in the time domain is that disturbances, of whether periodic, of tidal origin, or non-periodic, of meteorological origin such as wind stresses, storm surges, and other origin can be easily incorporated into calculations.

Another important fact is that in the formulation of LTE, the neglect of the nonlinear advective term, i.e. the convective rate of change of $\underset{\sim}{U}$ from its changing position in space as applied to numerical modeling of the tides and currents in the actual oceans, where $\underset{\sim}{U}$ is the particle velocity of water, has never been challenged. With a gradual change of the shape of continental boundaries and of the depth of water in the oceans, the convective rate of change of $\underset{\sim}{U}$ can be expected to be small in comparison with the local rate of change of $\underset{\sim}{U}$ at a fixed point. Nevertheless, when the shape of continental boundaries, particularly around the reentrant corners, for example, in the regions of Caribbean Sea and Gulf of Mexico/Cuba and Yucatan, New Zealand and Auckland Island Plateau in the southwestern Pacific Ocean, Iceland and Spitsbergen of the North Atlantic Ocean, Madagascar in the Indian Ocean, and many other reentrant corners, and the depth of water, particularly across trenches and continental margins, the convective rate of change of $\underset{\sim}{U}$ from its changing position in space may reach nearly a comparable order or only one order of magnitude less than the local rate of change of $\underset{\sim}{U}$ at a fixed point. That means in realistic modeling of the tides and currents in the actual oceans, therefore, we must consider the convective rate of change of $\underset{\sim}{U}$.

During the last decade or so, our major efforts at Columbia University on modeling ocean tides have been directed toward solving the time-domain total tides and currents not only for the global oceans but also for the coastal region, the continental shelf, the continental slope and the deep ocean as a complete system (Kuo et al, 1986a, b). In this paper, we shall present only the results of finite-element modeling of the global ocean tides and currents for the concurrent period of SEASAT in orbit, differing from the previous finite-difference models of the global ocean tides as follows:

1. As the fundamental governing equations for solving the tides and currents of the global oceans, we chose the vertically integrated hydrodynamic equations, or the shallow water equations, instead of the Laplace's Tide Equations used by other modelers in the past. That means the nonlinear advective term, or the convective rate of change of $\underset{\sim}{U}$ from its changing position in space, is included.
2. We model the tides and currents of the global oceans on an elastic Earth in the time domain to obtain the total tides and currents, as astronomically forced by the Moon and the Sun so that the variation of tide and current is a function of time and space, instead of in the frequency domain or a single frequency, as done by other modelers in the past.

3. We use the finite element method instead of the finite difference method as used in the past by other modelers that permits us to use variable element grid sizes. In the present case, the ratio of the smallest to the largest element grid-size is 1:5,000, enabling us to better model the rapid change of water depth across trenches and continental margins, and high irregularity of continental boundaries.
4. We use the semi-implicit time integration method. This allows to take advantage of large time steps for a stable and fast numerical convergence.
5. Our finite-element modeling results of the tides and currents of the global oceans strictly represent the response of the oceans to the tidal generating forces of the Moon and the Sun and are not constrained by tidal gauge observations anywhere in the calculation.

Finally, we present here a comparison of our finite-element results of the total tides of the global oceans with the data of SEASAT to illustrate the reliability of our finite-element method for modeling the tides and currents in the global oceans.

## Basic Finite-Element Formulation

The time-domain vertically integrated hydrodynamic equations or so called shallow-water equations and the equation of continuity in the spherical coordinate system are explicitly given by (Kuo, 1987)

$$\begin{aligned}
&\partial u_\Theta/\partial t + u_\Theta/a(\partial u_\Theta/\partial\Theta) + u_\lambda/(a\cos\Theta)\,(\partial u_\Theta/\partial\lambda) - 2\Omega\sin\Theta\, u_\lambda \\
&\quad + g/a(\partial\zeta/\partial\Theta) + k_b|u|/H u_\Theta - f_\Theta - W_\Theta = 0 \\
&\partial u_\lambda/\partial t + u_\Theta/a(\partial u_\lambda/\partial\Theta) + u_\lambda/(a\cos\Theta)\,(\partial u_\lambda/\partial\lambda) - 2\Omega\sin\Theta\, u_\Theta \\
&\quad + g/(a\cos\Theta)\,(\partial\zeta/\partial\lambda) + k_b|u|/H u_\lambda - f_\Theta - W_\Theta = 0 \\
&\partial\zeta/\partial t + 1/(a\cos\Theta)\,\partial[(\zeta+h)u_\Theta\cos\Theta]/\partial\Theta \\
&\quad + 1/(a\cos\Theta)\,\partial[(\zeta+h)u_\lambda]/\partial\lambda = 0
\end{aligned} \tag{1}$$

where

$(\Theta,\lambda)$: $\Theta$ latitude and $\lambda$ longitude, positive in the west direction;
$(u_\Theta,u_\lambda)$: vertically averaged horizontal velocity;
a: the mean radius of the Earth;
$\Omega$: angular velocity of the Earth's rotation;
g: acceleration of gravity, 9.81 m/s$^2$;
$k_b$: bottom friction coefficient, generally taken to be equal to 0.003;
$(f_\Theta,f_\lambda)$: horizontal components of tide-generating force;
$(W_\Theta,W_\lambda)$: horizontal components of wind stress.
$\zeta$: tidal height measured from mean sea level with the axis taken positive upward;
$H = h+\zeta$ is the water-column thickness, where $h$ is the depth to the ocean bottom measured from mean sea level.

For the finite-element calculation, the north and the west horizontal components of the tide-generating force due to the Moon and the Sun are calculated according to

$$
\begin{aligned}
f_\Theta = {} & [3\mu M r^2/(2d^4)\,(5\cos^2 Z_m - 1) + 3\mu M r/d^3 \cos Z_m]\,(-\sin Z_m \mathrm{d}Z_m/\mathrm{d}\Theta) \\
& + 3\mu S r/D^3 \cos Z_s\,(-\sin Z_s \mathrm{d}Z_s/\mathrm{d}\Theta) \\
f_\lambda = {} & (1/\cos\Theta)\,[3\mu M r/d^3 \cos Z_m + 3\mu M r^2/(2d^4)\,(5\cos^2 Z_m - 1)] \\
& (-\sin Z_m \mathrm{d}Z_m/\mathrm{d}\lambda) + (1/\cos\Theta)\,[3\mu S r/D^3 \cos Z_s]\,(-\sin Z_s \mathrm{d}Z_s/\mathrm{d}\lambda)
\end{aligned}
\tag{2}
$$

where

$$
\begin{aligned}
-\sin(Z_m)\,\mathrm{d}Z_m/\mathrm{d}\Theta &= f_1(\Theta, I, l, \chi) \\
-\sin(Z_s)\,\mathrm{d}Z_s/\mathrm{d}\Theta &= f_1(\Theta, \omega, l_1, \chi_1) \\
-\sin(Z_m)\,\mathrm{d}Z_m/\mathrm{d}\lambda &= f_2(\Theta, I, l, \chi) \\
-\sin(Z_s)\,\mathrm{d}Z_s/\mathrm{d}\lambda &= f_2(\Theta, \omega, l_1, \chi_1)
\end{aligned}
$$

with

$$
\begin{aligned}
f_1(\Theta, I, l, \chi) = {} & \cos\Theta \sin I \sin l \\
& -\sin\Theta[\cos^2(I/2)\cos(l-\chi) + \sin^2(I/2)\cos(l+\chi)] \\
f_2(\Theta, I, l, \chi) = {} & \cos\Theta[\sin^2(I/2)\sin(l+\chi) \\
& -\cos^2(I/2)\sin(l-\chi)]
\end{aligned}
$$

and

$d$: distance between the centers of the Earth and the Moon;
$D$: distance between the centers of the Earth and the Sun;
$r$: distance between the center of the Earth and the observation point;
$Z_m$: zenith angle of the Moon;
$Z_s$: zenith angle of the Sun;
M: mass of the Moon;
S: mass of the Sun;
$\mu$: gravitational constant;
$I$: inclination of the Moon's orbit to the equator;
$\omega$: inclination of the Earth's equator to the ecliptic;
$l$: longitude of the Moon in its orbit reckoned from its ascending intersection with the equator;
$l_1$: longitude of the Sun in the ecliptic reckoned from the vernal equinox;
$\chi$: right ascension of the meridian of the observation-point reckoned from the ascending intersection of the Moon's orbit with the equator;
$\chi_1$: right ascension of the meridian of the observation point reckoned from the vernal equinox.

The dependent variables $(u_\Theta, u_\lambda, \zeta)$ and the depth $h$ are approximated by a linear combination of localized basis as follows:

$$
\begin{aligned}
u_\Theta(\Theta,\lambda,t) &= N_k(\Theta,\lambda)\, q_{\Theta,k}(t) \\
u_\lambda(\Theta,\lambda,t) &= N_k(\Theta,\lambda)\, q_{\lambda,k}(t) \\
\zeta(\Theta,\lambda,t) &= N_k(\Theta,\lambda)\, \xi_k(t) \\
h(\Theta,\lambda) &= N_k(\Theta,\lambda)\, \hat{h}_k \\
f_\Theta(\Theta,\lambda,t) &= N_k(\Theta,\lambda)\, \hat{f}_{\Theta,k}(t) \qquad W_\Theta(\Theta,\lambda,t) = N_k(\Theta,\lambda)\, \hat{w}_{\Theta,k}(t) \\
f_\lambda(\Theta,\lambda,t) &= N_k(\Theta,\lambda)\, \hat{f}_{\lambda,k}(t) \qquad W_\lambda(\Theta,\lambda,t) = N_k(\Theta,\lambda)\, \hat{w}_{\lambda,k}(t)
\end{aligned}
\tag{3}
$$

where $N_k$ is the element's shape function of the $k$-th node. Substituting the above nodal functions (3) into the differential equations (1) we have

$$
\begin{aligned}
&\alpha_{jk}[(q_{\Theta,k}^{t+1}-q_{\Theta,k}^{t-1})/(2\Delta t)]-\omega_{jk}[(q_{\lambda,k}^{t+1}+q_{\lambda,k}^{t-1})/2]+\gamma_{\Theta,jk}[(\xi_k^{t+1}+\xi_k^{t-1})/2]\\
&\quad=-\beta_{jk}(q_{\Theta,i}^{t}, q_{\lambda,i}^{t})\, q_{\Theta,k}^{t}-\mathrm{k_b}\,\varepsilon_{jk}(\psi_i^{t-1})\, q_{\Theta,k}^{t-1}+\alpha_{jk}\hat{f}_{\Theta,k}^{t}+\alpha_{jk}\hat{w}_{\Theta,k}^{t}\\
&\alpha_{jk}[(q_{\lambda,k}^{t+1}-q_{\lambda,k}^{t-1})/(2\Delta t)]+\omega_{jk}[(q_{\Theta,k}^{t+1}+q_{\Theta,k}^{t-1})/2]+\gamma_{\lambda,jk}[(\xi_k^{t+1}+\xi_k^{t-1})/2]\\
&\quad=-\beta_{jk}(q_{\Theta,i}^{t}, q_{\lambda,i}^{t})\, q_{\lambda,k}^{t}-\mathrm{k_b}\,\varepsilon_{jk}(\psi_i^{t-1})\, q_{\lambda,k}^{t-1}+\alpha_{jk}\hat{f}_{\lambda,k}^{t}+\alpha_{jk}\hat{w}_{\lambda,k}^{t}\\
&\alpha_{jk}[(\xi_k^{t+1}-\xi_k^{t-1})/(2\Delta t)+\delta_{\Theta,jk}(\hat{h}_i)[(q_{\Theta,k}^{t+1}+q_{\Theta,k}^{t-1})/2]+\\
&\quad+\delta_{\lambda,jk}(\hat{h}_i)[(q_{\lambda,k}^{t+1}+q_{\lambda,k}^{t-1})/2]=-\delta_{\Theta,jk}(\xi_i^{t})\, q_{\Theta,k}^{t}-\delta_{\lambda,jk}(\xi_i^{t})\, q_{\lambda,k}^{t}
\end{aligned}
\tag{4}
$$

where the superscript $t$ is for the $n$-th time step, and

$$
\begin{aligned}
\alpha_{jk} &= \sum_e \iint N_j N_k \cos\Theta \,\mathrm{d}\Theta\,\mathrm{d}\lambda\\
\omega_{jk} &= \sum_e \iint 2\Omega N_j N_k \sin\Theta\cos\Theta \,\mathrm{d}\Theta\,\mathrm{d}\lambda\\
\gamma_{\Theta,jk} &= \sum_e \iint \mathrm{g/a}\ (\partial N_k/\partial\Theta) N_j \cos\Theta \,\mathrm{d}\Theta\,\mathrm{d}\lambda\\
\gamma_{\lambda,jk} &= \sum_e \iint \mathrm{g/a}\ (\partial N_k/\partial\lambda) N_j \,\mathrm{d}\Theta\,\mathrm{d}\lambda\\
\beta_{jk} &= \sum_e \iint [N_i q_{\Theta,i}(\partial N_k/\partial\Theta)\cos\Theta + N_i q_{\lambda,i}(\partial N_k/\partial\lambda)] N_j/\mathrm{a}\ \,\mathrm{d}\Theta\,\mathrm{d}\lambda\\
\varepsilon_{jk}(\psi_i) &= \sum_e \iint N_j N_k N_i [(q_{\Theta,i}^2+q_{\lambda,i}^2)^{1/2}/(\hat{h}_i+\xi_i)]\cos\Theta \,\mathrm{d}\Theta\,\mathrm{d}\lambda\\
\delta_{\Theta,jk}(\hat{h}_i) &= \sum_e \iint 1/\mathrm{a}\ [\partial(N_k N_i \hat{h}_i\cos\Theta)/\partial\Theta] N_j \,\mathrm{d}\Theta\,\mathrm{d}\lambda\\
\delta_{\lambda,jk}(\hat{h}_i) &= \sum_e \iint 1/\mathrm{a}\ [\partial(N_k N_i \hat{h}_i)/\partial\lambda] N_j \,\mathrm{d}\Theta\,\mathrm{d}\lambda.
\end{aligned}
\tag{5}
$$

In equations (5), summation is taken over all elements in the domain of consideration.

Because the basis functions have only local support, the values of the integrals in (5) are nonzero only for the elements containing the indicated nodes with the result that the matrices are sparse and banded.

Rearranging (4) and denoting the transpose of the vector

$$(q_{\Theta 1}, q_{\lambda 1}, \xi_1, q_{\Theta 2}, q_{\lambda 2}, \xi_2, \ldots, q_{\Theta n}, q_{\lambda n}, \xi_n)$$

by $Q$, where n is the total number of nodes in the computing domain, we can express (4) in matrix form as follows:

$$\tilde{L}^* Q^{t+1} = \tilde{M}^* Q^{t-1} - \tilde{P}^* Q^t - \tilde{S}^* Q^{t-1} \tag{6}$$

where the matrices $\tilde{L}^*, \tilde{M}^*, \tilde{P}^*, \tilde{S}^*$ are large $(3n \times 3n)$, sparse, banded matrices.

For ease in treating the irregular boundaries that arise from consideration of realistic geometries and for implementing rigid-wall boundary conditions, it is convenient to

make a coordinate transformation before the final global assembly of (6). Applying the transformation to (6), we get

$$\tilde{L}Q^{t+1} = \tilde{M}Q^{t-1} - \tilde{P}Q^{t} - \tilde{S}Q^{t-1} \tag{7}$$

where $\tilde{L} = R^T \tilde{L}^* R$; $\tilde{M} = R^T \tilde{M}^* R$; $\tilde{P} = R^T \tilde{P}^* R$; $\tilde{S} = R^T \tilde{S}^* R$ and where $R$ and $R^T$ are the diagonal matrices, containing the rotational and the transposed submatrices.

The basis functions ($N_i$) used in this model are the linear members of the isoparametric serendipity family defined at the four corners of a square element of side length 2 in a $\xi$-$\eta$ coordinate system to be (Zienkiewicz, 1977):

$$N_i = 1/4 \ (1 + \xi\xi_i)\ (1 + \eta\eta_i) \quad \text{for } (\xi_i, \eta_i) = (\pm 1, \pm 1).$$

The integrals of products of basis functions and their derivatives are obtained by mapping the element coordinates from the global $\Theta$-$\lambda$ system into the $\xi$-$\eta$ coordinate system and then performing the integration numerically using Gauss-Legendre quadrature. The mapping is unique for linear elements, provided no internal angles are greater than 180° (Zienkiewicz, 1977).

As the latitude for the ocean region approaches that of the polar region, as in the case of the Arctic Ocean, the spherical coordinates have a singular point at the north pole, where the longitudes converge to one point. To overcome this singularity problem, we choose a local rectangular coordinate system in the finite-element formulation to carry out the calculation needed for each element. The finite-element formulation in the local $x$- and $y$-coordinate system can be found in Malone and Kuo (1981), in which a unified local coordinate system is used for all elements, because the area under consideration is small, on the order of several degrees in both latitude and longitude (Kuo et al, 1986b).

## Finite-Element Results of Tides and Currents

As pointed out and shown by Kuo et al (1986b) and Kuo (1987), the spatial discretization of the information contained in the bathymetric data base of the world oceans is undoubtedly of great importance in achieving the accuracy of the later finite-element calculation. For this very reason, the $1° \times 1°$ bathymetric data of the world oceans were recontoured. The recontoured map was then used to discretize the world oceans with variable quadrilateral-element sizes. The rigid-boundary conditions of all the oceans were imposed at a depth of 1000 m, except off New Zealand, where a depth of 500 m was used, and off Spitsbergen where the depth was less than 500 m. Because of convenience in the polar regions, the Miller projection, given by

$$\Theta = 5/2\ (\tan^{-1}[\exp(4Y/5)] - \pi/4),$$

where $Y$ is the latitude of the projection, was adopted.

The total number of nodal points for the world oceans is 9274, including 1467 for the Atlantic, 1867 for the Indian, 4443 for the Pacific, and 1497 for the Arctic Oceans.

Figure 1 shows the finite-element spatial discretization of the world oceans with the variable grid shaded to indicate depth. With three degrees of freedom for each nodal point, there are thus 27,822 equations to be solved in matrix form.

The interaction of the earth tide and the ocean tide is approximately corrected for in a fashion similar to that described by Pekeris (1978) and Schwiderski (1980a, 1980b).

Every precaution was taken concerning the problems one is confronted with when modeling tides and currents, namely

1. time integration of the initial weak coupling of the equations of motion and the continuity equation,
2. numerically adequate resolution around reentrant corners in various parts of the oceans and
3. a cold-start initial condition.

It was found that the time integration can be relaxed to either 30 minutes or one hour per step; a 30-minute time step was adopted in order to insure the accuracy of the calculation. The tidal generating forces of the Moon and the Sun were calculated according to equation (2), i.e., up to the third order of Legendre polynomial for the Moon and to the second order for the Sun.

Figures 2 through 13 show the tidal generating forces, the total tide-induced currents, and the total tidal heights as a function of space and time every three hours, beginning 00:00:00 GMT, 22 September 1978, during which time SEASAT was in orbit. The finite-element results of the total tides and the total currents for the global oceans reveal the intricacy and complexity of the general circulation of the oceans due to the tidal generating forces, particularly along the irregular ocean boundaries, islands, narrow straits, and gulfs. The distinctive patterns of tidal currents and tidal heights for the world oceans interconnected, as shown in Figures 2 through 13, result from the interflow of the tide-induced currents which, in turn, modify the tidal heights throughout the world oceans. Moreover, the interflow of the tide-induced currents between the Pacific and Indian Oceans, and between the Atlantic and Arctic Oceans, has a profound influence on the general tidal circulation as a function of time and space.

## Comparison of the Tide Model Results with SEASAT Data

The SEASAT-1 altimeter data were provided to us by Choy and Grunes (1986), who compared the Schwiderski's tidal model and our finite-element regional tidal model of the Pacific Ocean with the SEASAT data. These data of SEASAT-1 had been preprocessed by the Naval Surface Weapons Center (NSWC) into the NSWC Geophysical Data Record Format (West, 1981). Uncertainties of the SEASAT satellite orbital determination and the available geoid model in the Gulf of Alaska region were greater than the tidal signals to make a comparison of tidal models with SEASAT data from a single pass over the ocean unprofitable. However, since the geoid is virtually time invarient in the time span of the orbit in question, a temporal change of sea surface height along the track thus has been obtained by differencing the altimeter height data of two passes


*Fig. 1: Finite-element discretization of the world oceans with bathymetric depths shaded as indicated in the key.*

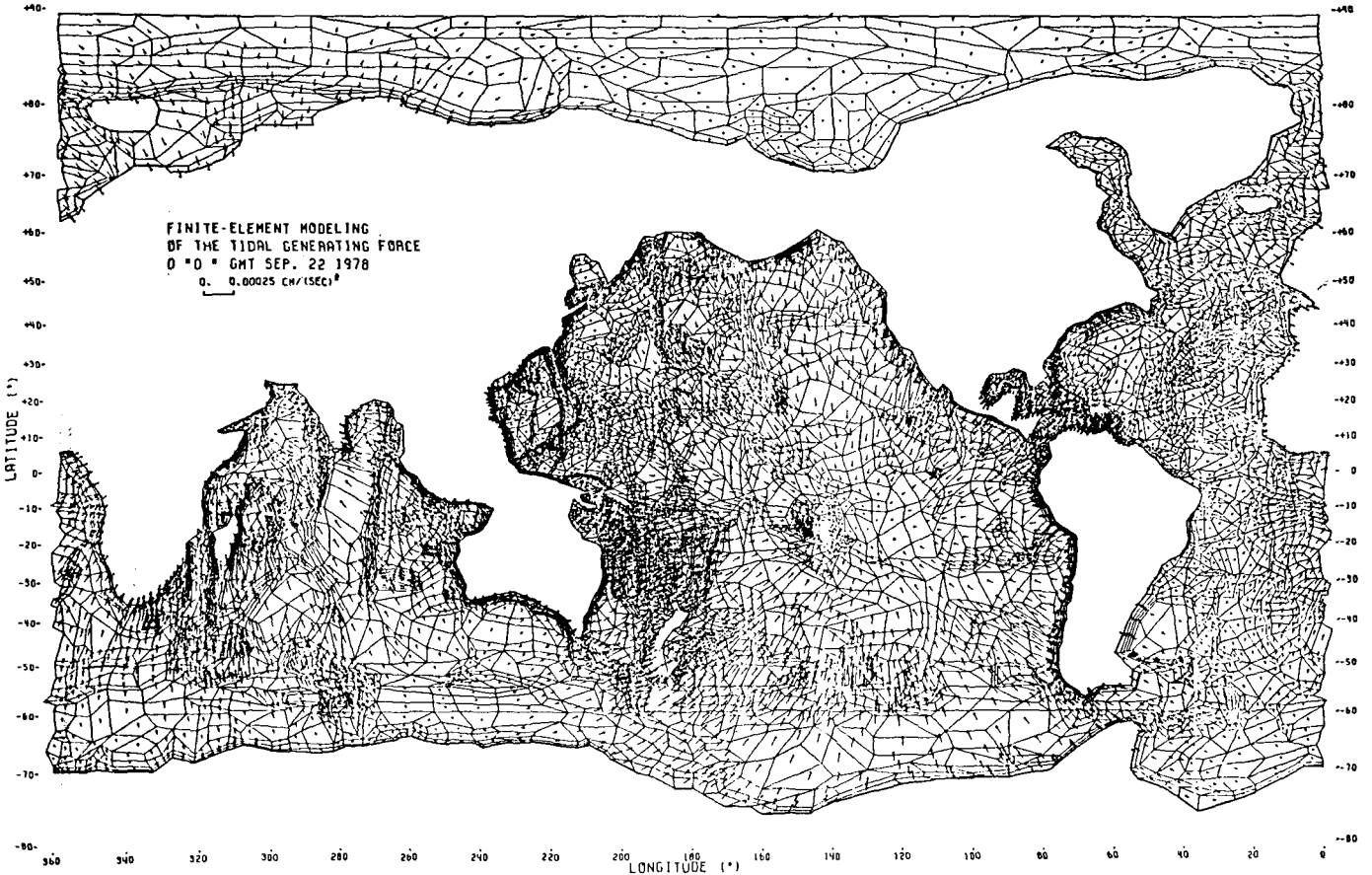


*Fig. 2: Finite-element modeling of the tidal generating forces at $0^h0^m$ GMT, September 22, 1978.*

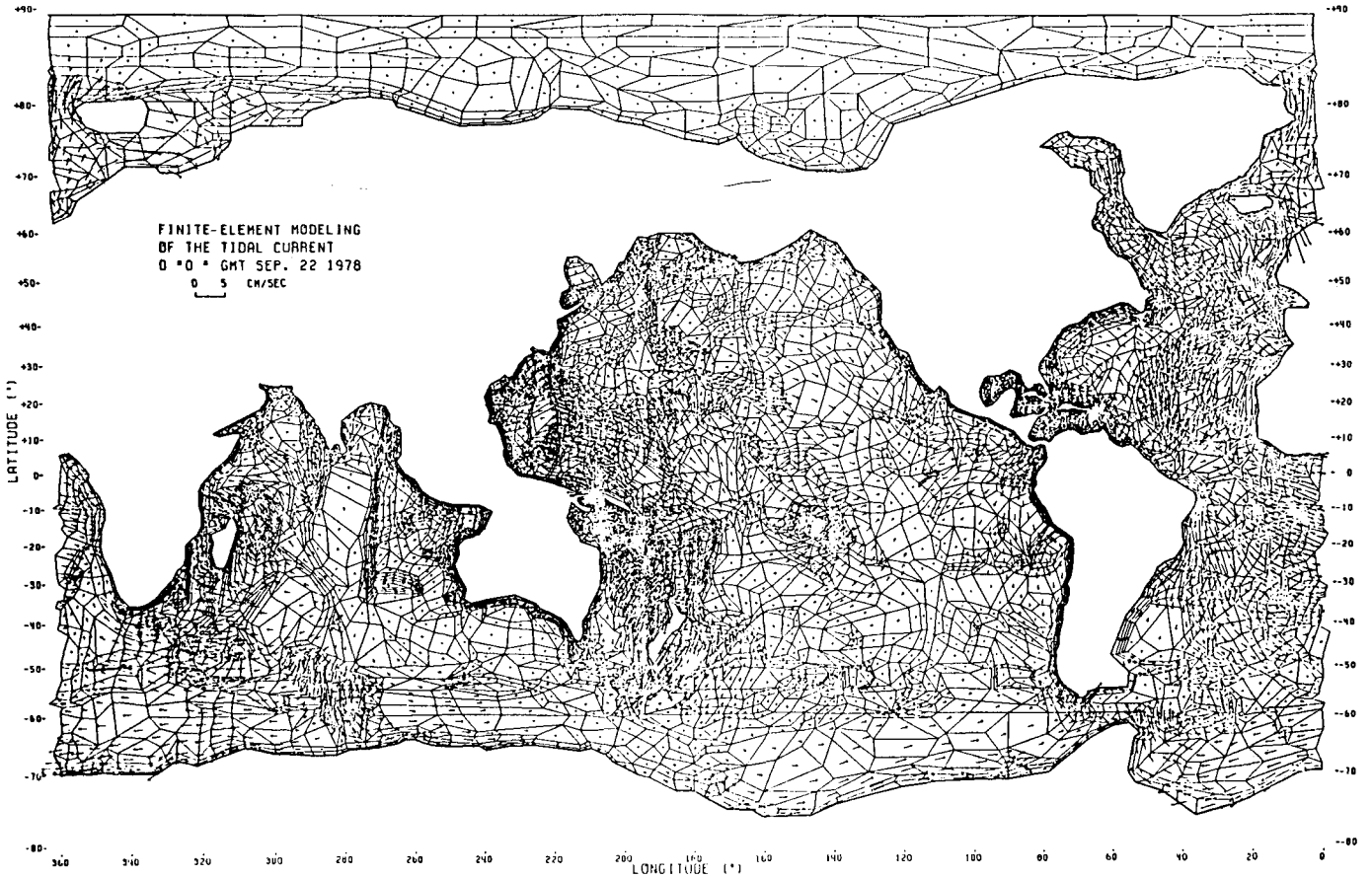


*Fig. 3: Finite-element modeling of the tidal current at $0^h0^m$ GMT, September 22, 1978.*

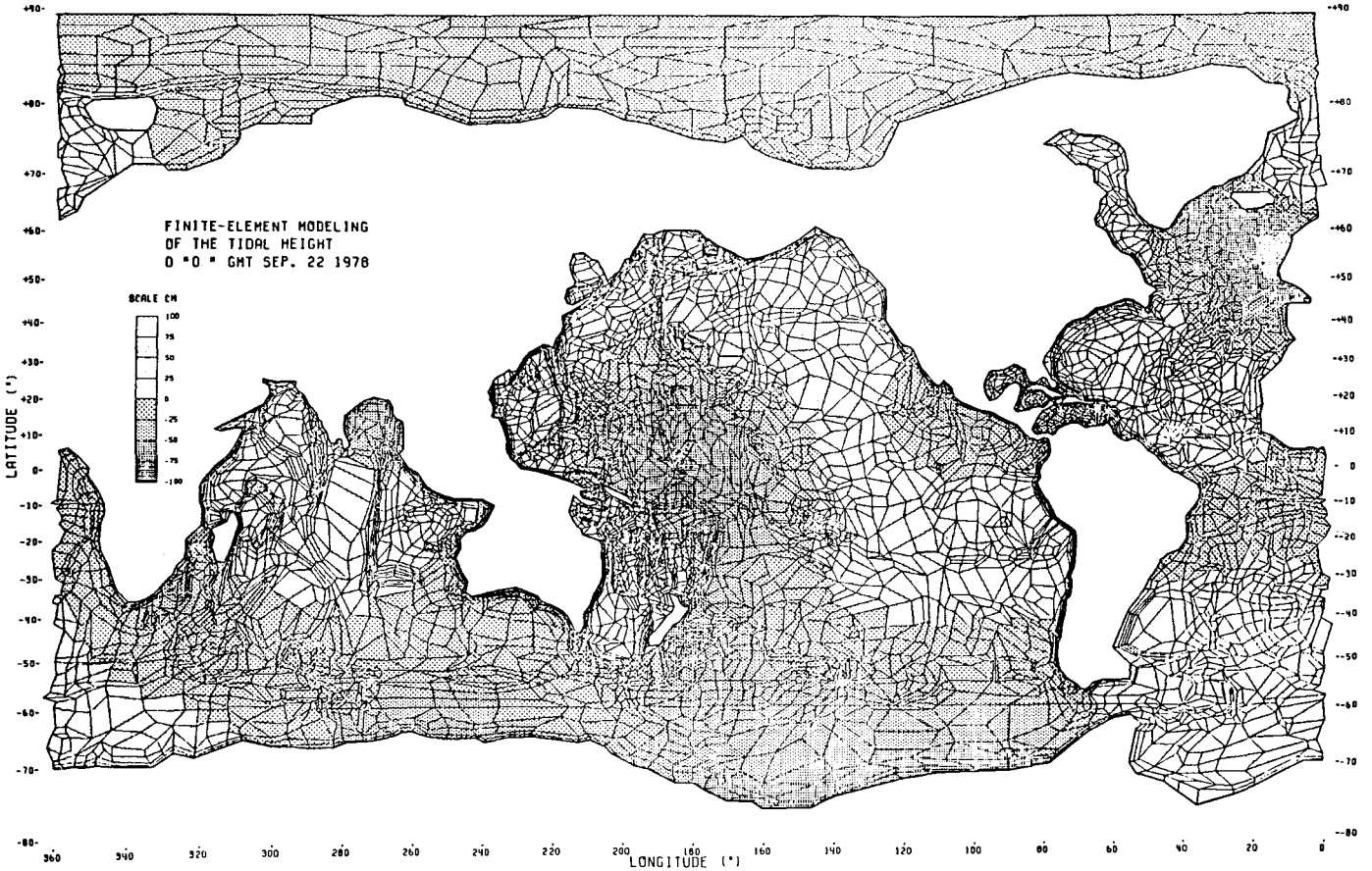


*Fig. 4: Finite-element modeling of the tidal height at $0^h0^m$ GMT, September 22, 1978.*

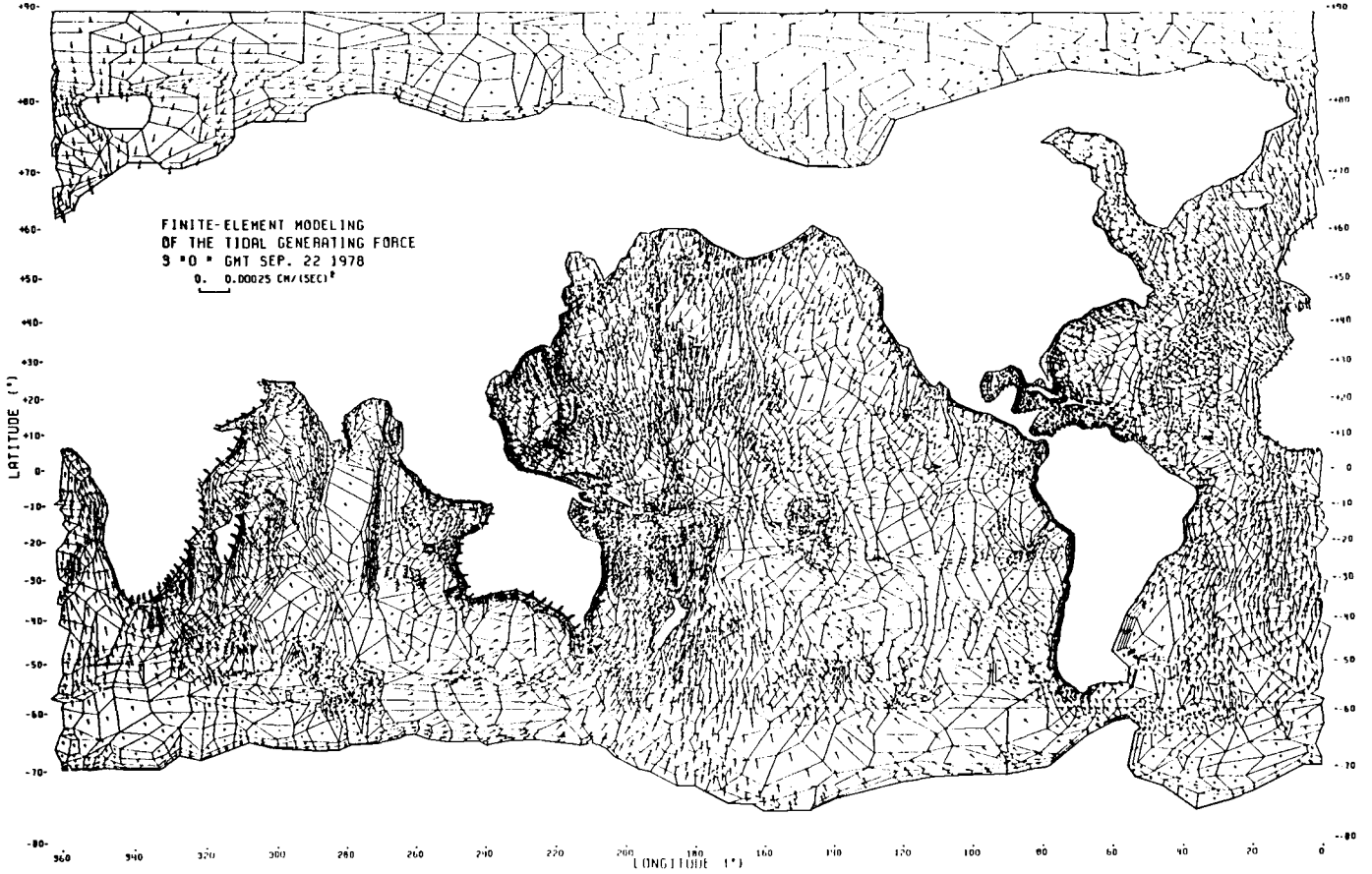


*Fig. 5: Finite-element modeling of the tidal generating forces at $3^h0^m$ GMT, September 22, 1978.*

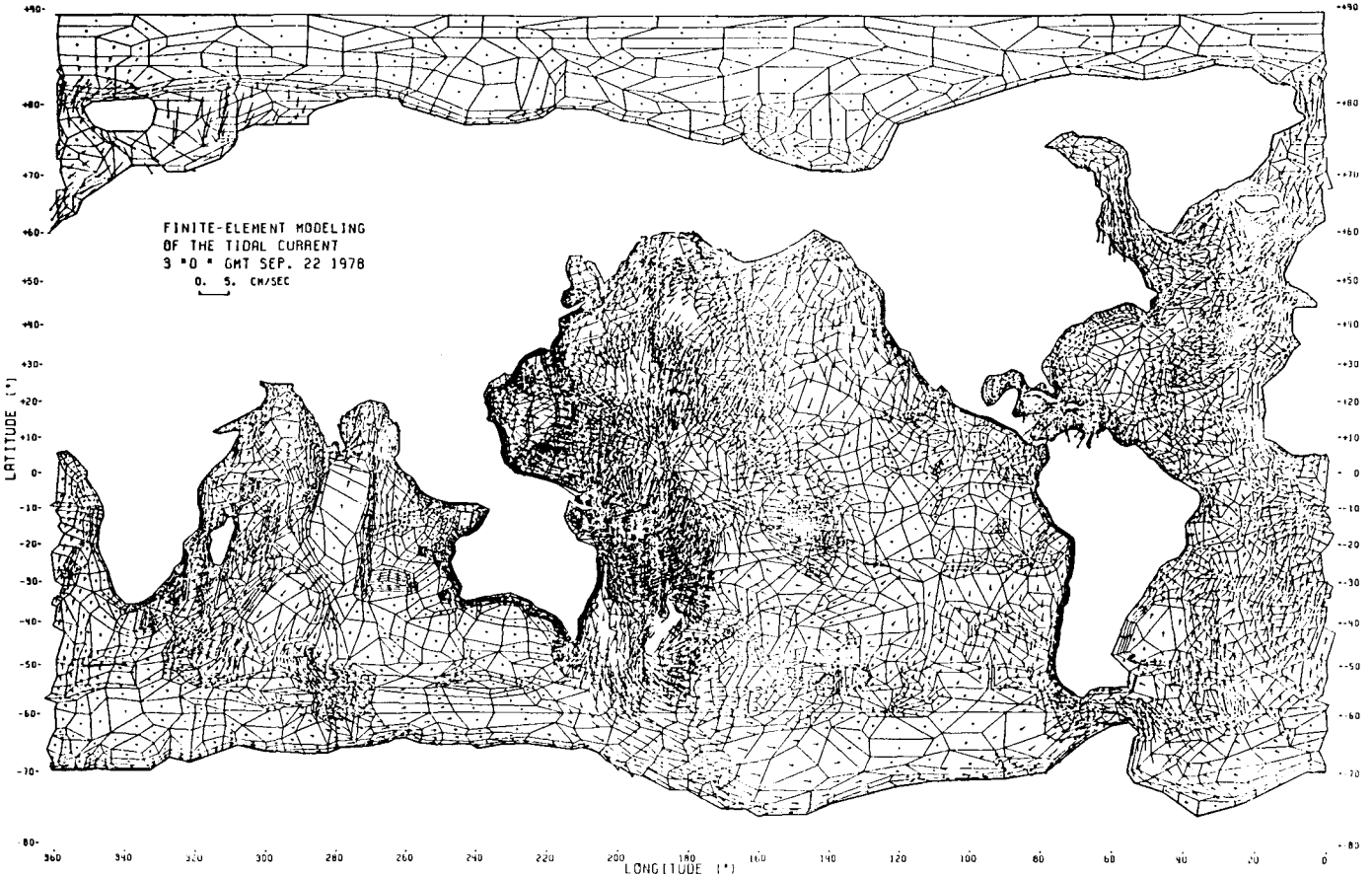


*Fig. 6: Finite-element modeling of the tidal current at $3^h0^m$ GMT, September 22, 1978.*

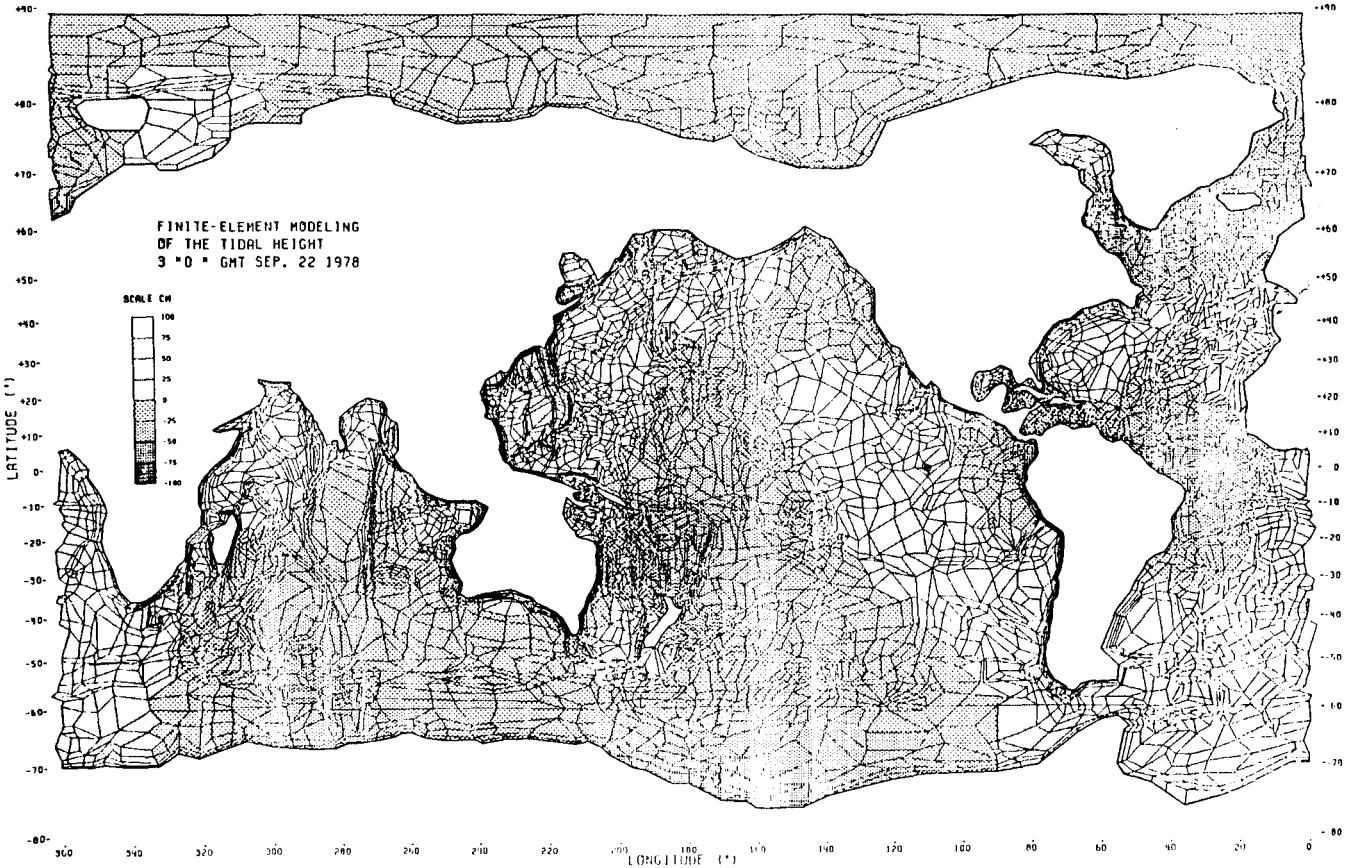


*Fig. 7: Finite-element modeling of the tidal height at $3^h0^m$ GMT, September 22, 1978.*

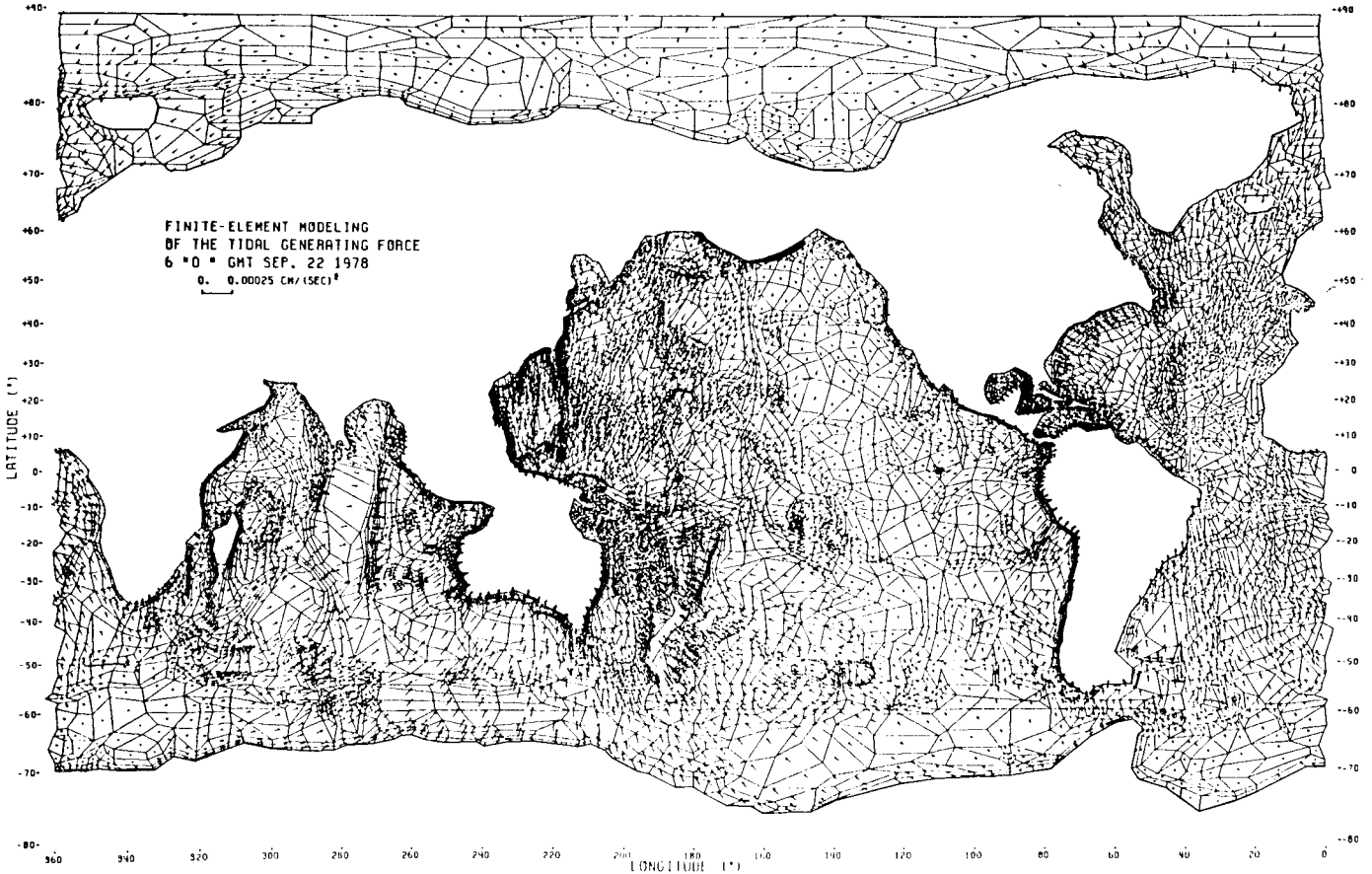


*Fig. 8: Finite-element modeling of the tidal generating forces at $6^h0^m$ GMT, September 22, 1978.*

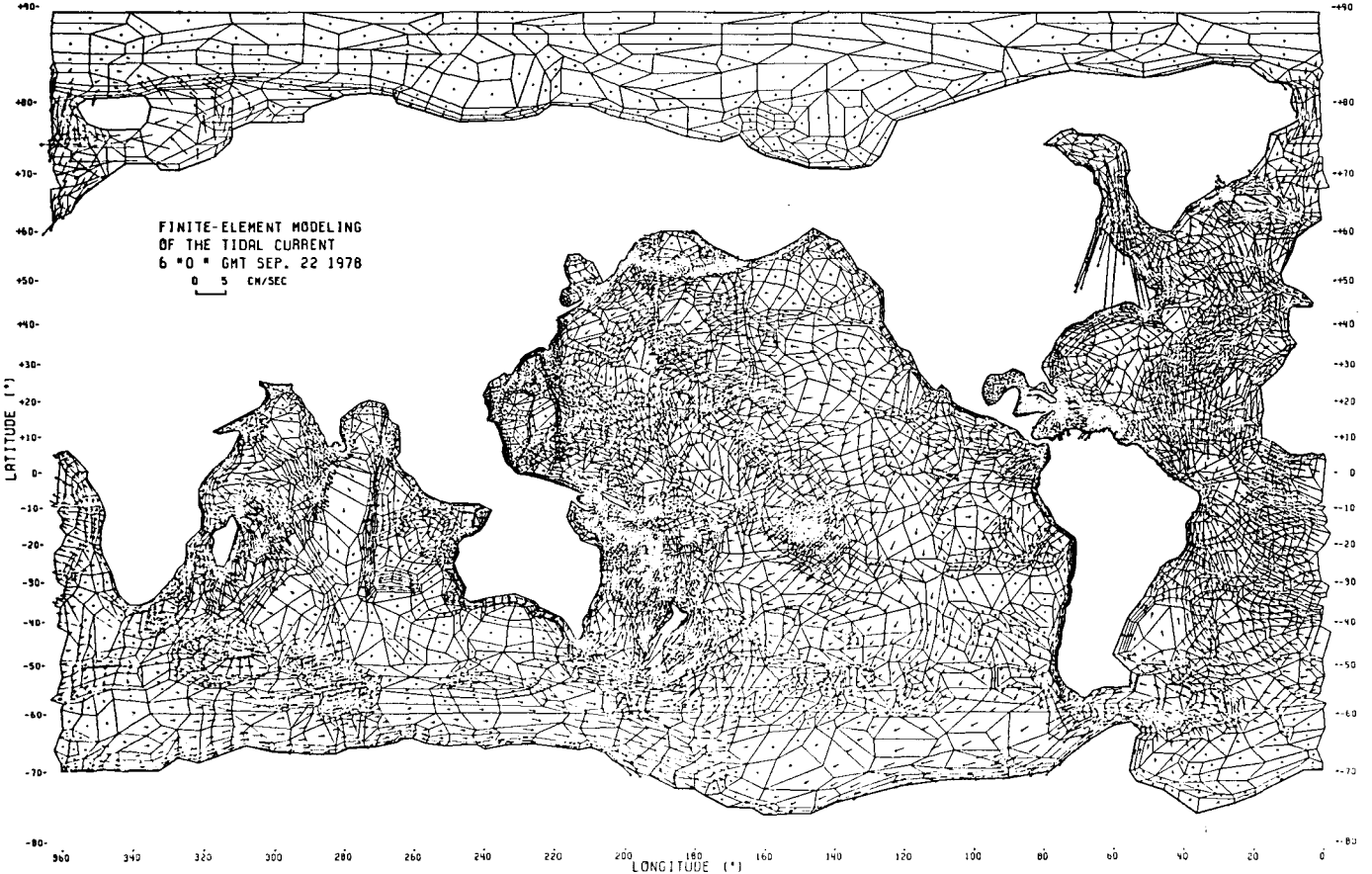


*Fig. 9: Finite-element modeling of the tidal current at $6^h0^m$ GMT, September 22, 1978.*

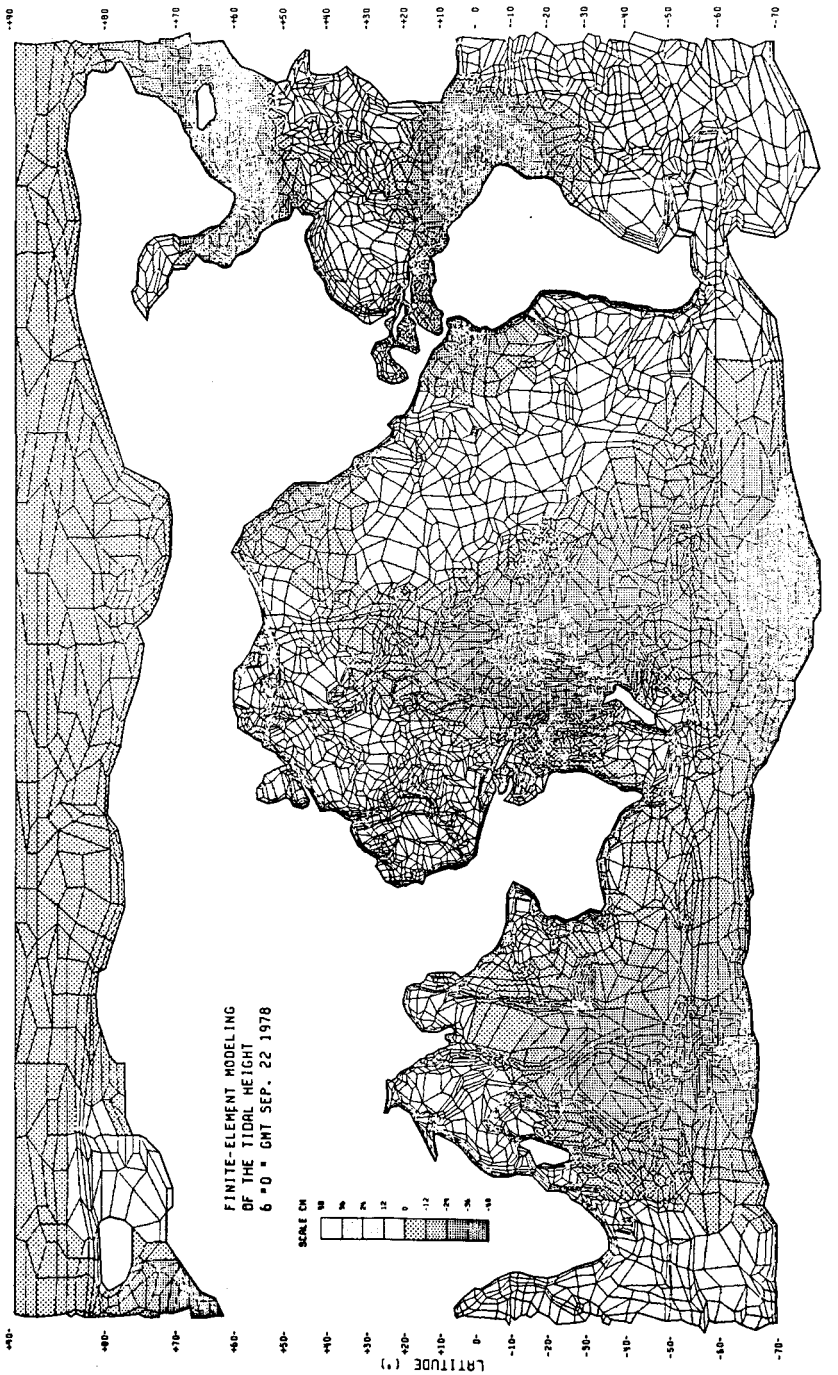


*Fig. 10: Finite-element modeling of the tidal height at $6^h0^m$ GMT, September 22, 1978.*

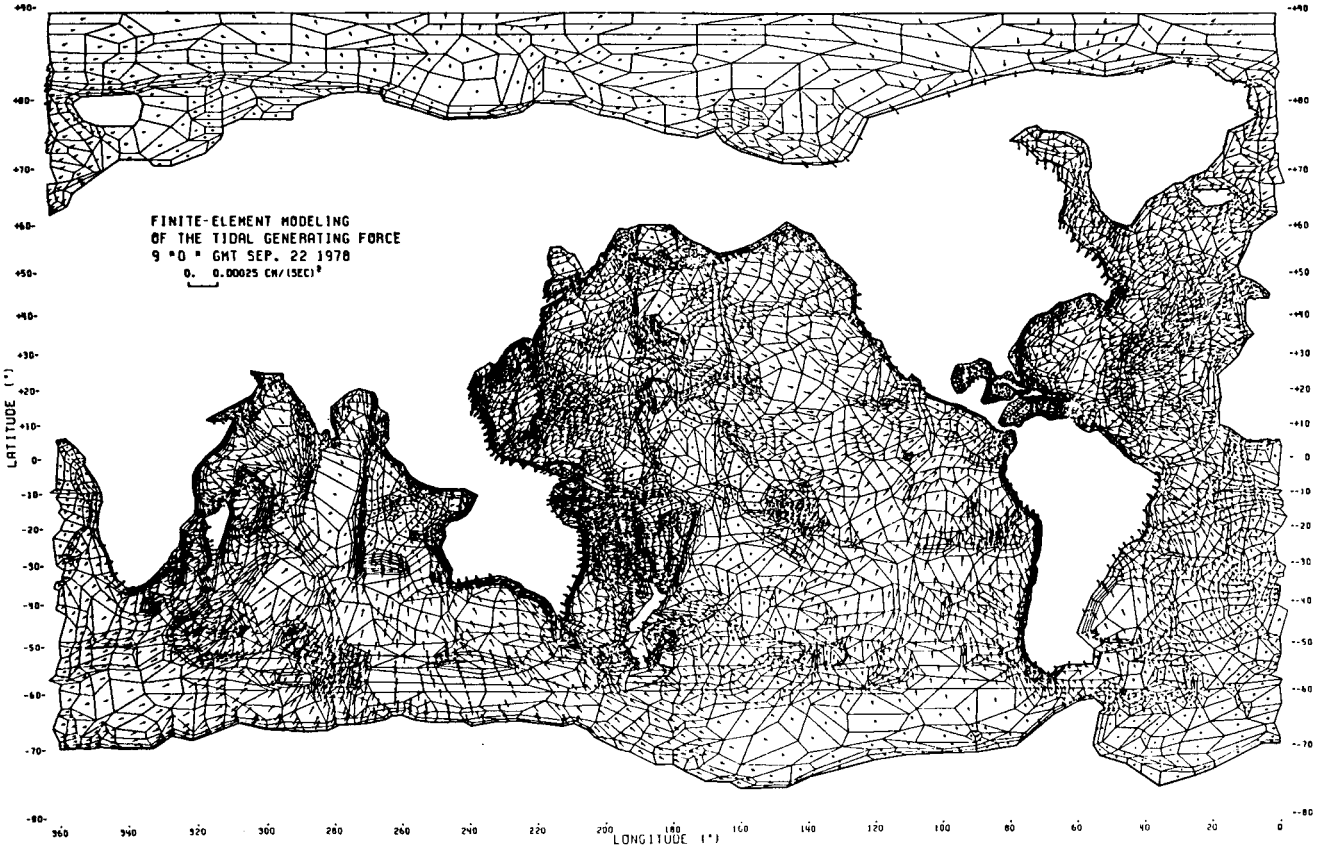


*Fig. 11: Finite-element modeling of the tidal generating forces at $9^h0^m$ GMT, September 22, 1978.*

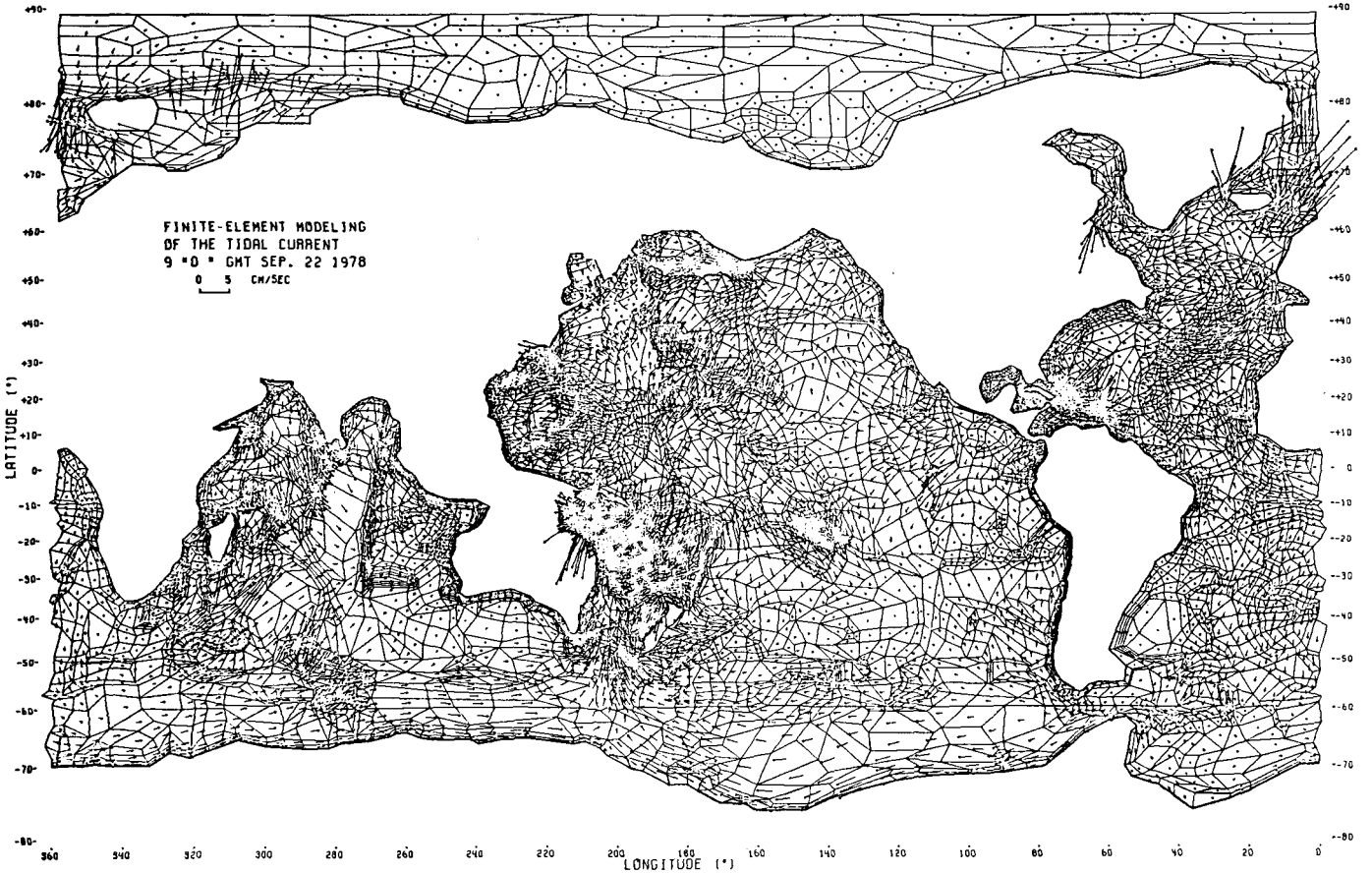


*Fig. 12: Finite-element modeling of the tidal current at $9^h0^m$ GMT, September 22, 1978.*

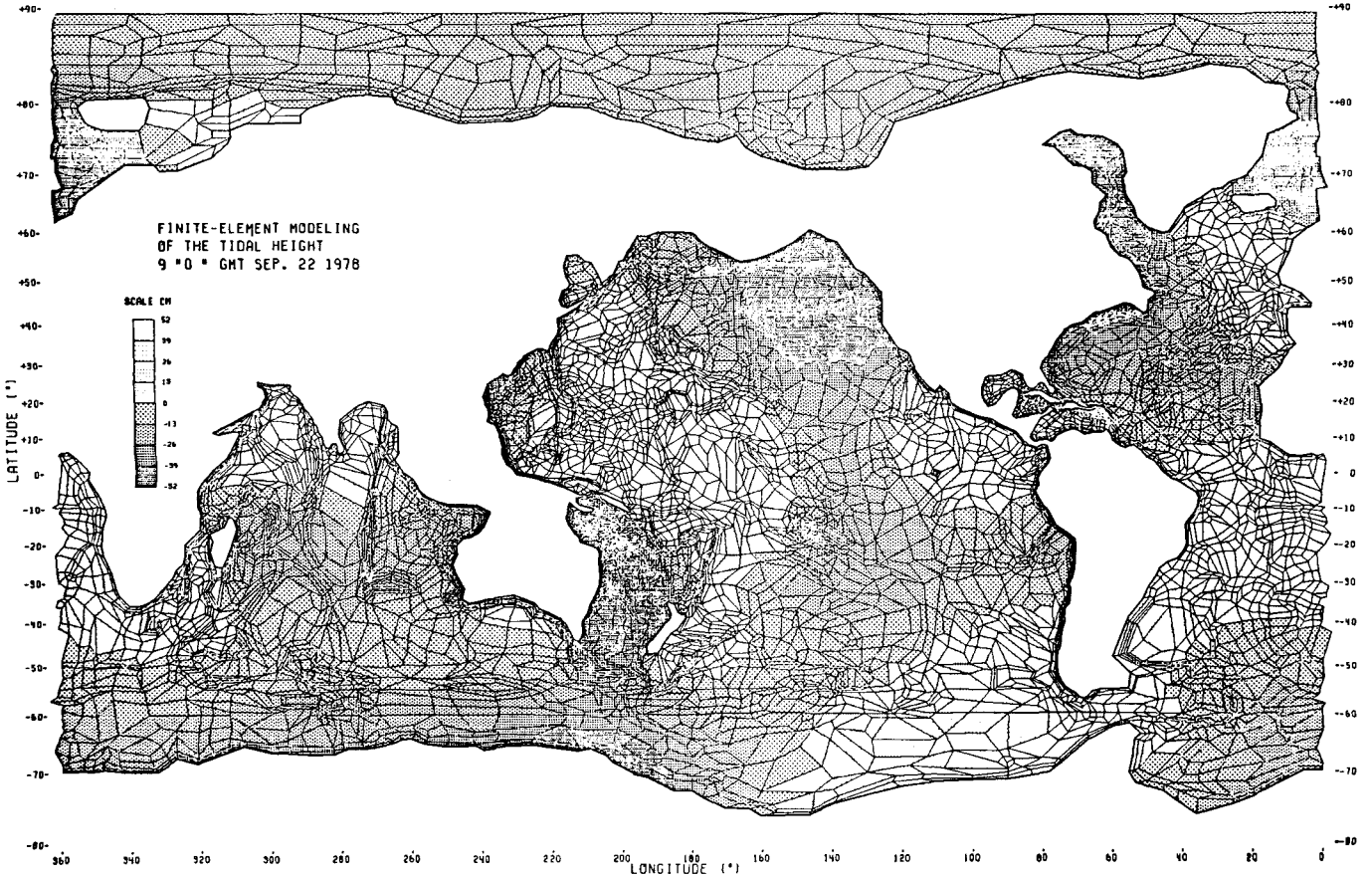


*Fig. 13: Finite-element modeling of the tidal height at $9^h0^m$ GMT, September 22, 1978.*

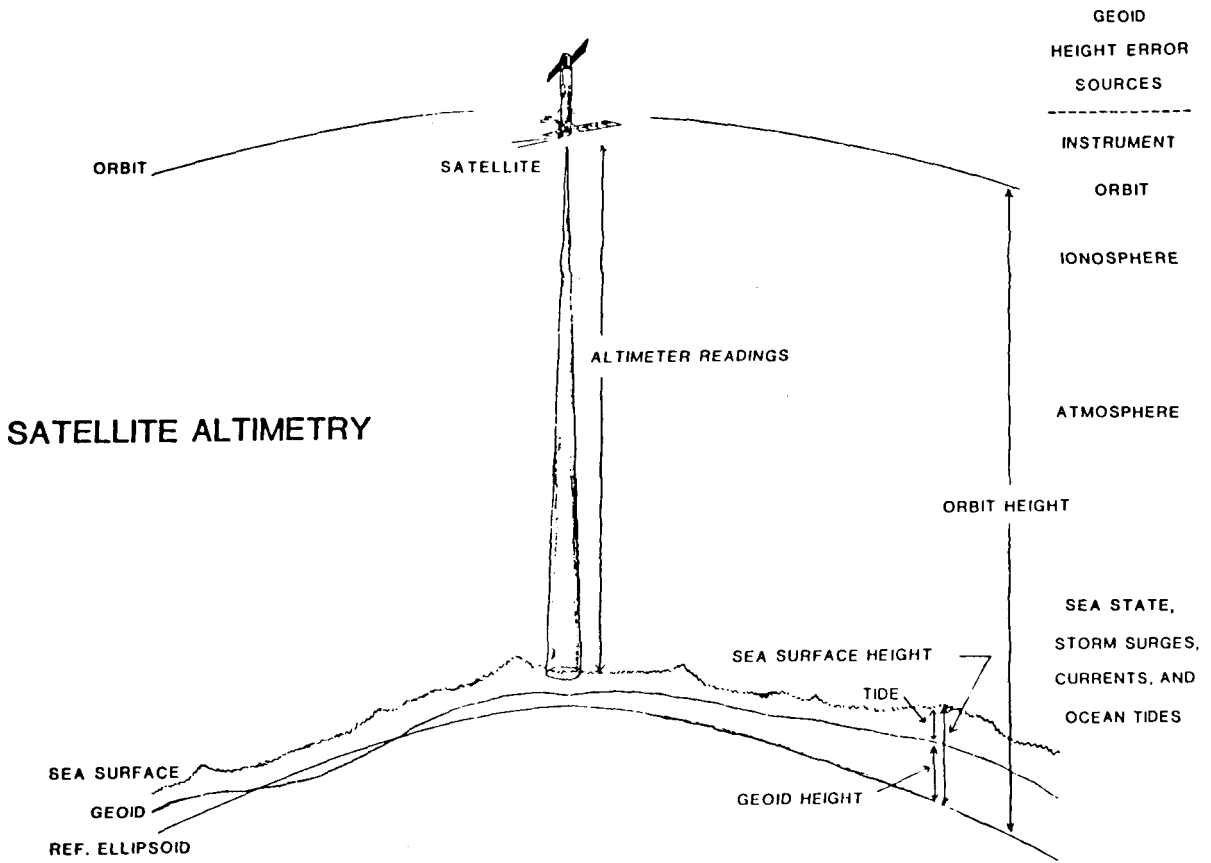


*Fig. 14: Satellite altimetry observation configuration (After Choy and Grunes, 1986).*

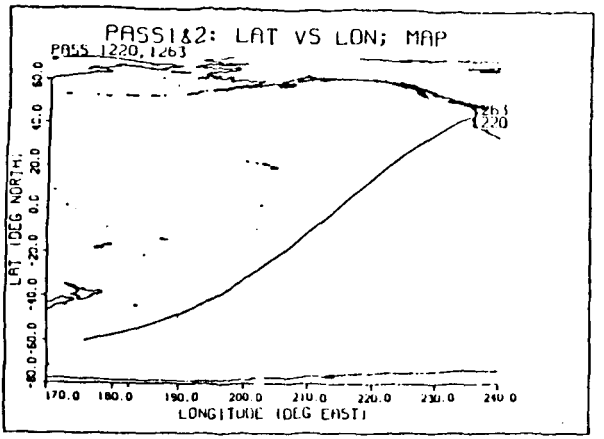


*Fig. 15: SEASAT orbital trajectory for passes 1220 and 1263 (a) and passes 1235 and 1278 (b). (After Choy and Grunes, 1986).*

over an identical ground track by Choy and Grunes (1986). Moreover, in order to minimize the long wavelength orbital error, Choy and Grunes chose a long segment of a pass (about one third of a revolution), and subtracted a second order polynomial least-squares fit with respect to time from the altimeter height difference data.

Figure 14 shows the observational configuration of satellite altimeter over the ocean. Figures 15a and 15b show the SEASAT orbital trajectory for the sub-satellite tracks of passes 1220 and 1263, and passes 1235 and 1278, respectively.

Figures 16a and 16b are the comparisons of the sea surface height differences among the SEASAT-1 altimeter data after the above mentioned re-processing by Choy and Grunes, the Schwiderski's tidal model (Schwiderski, 1980c; Schwiderski and Szeto, 1981), and our finite-element global tidal model for passes 1220 and 1263, and passes

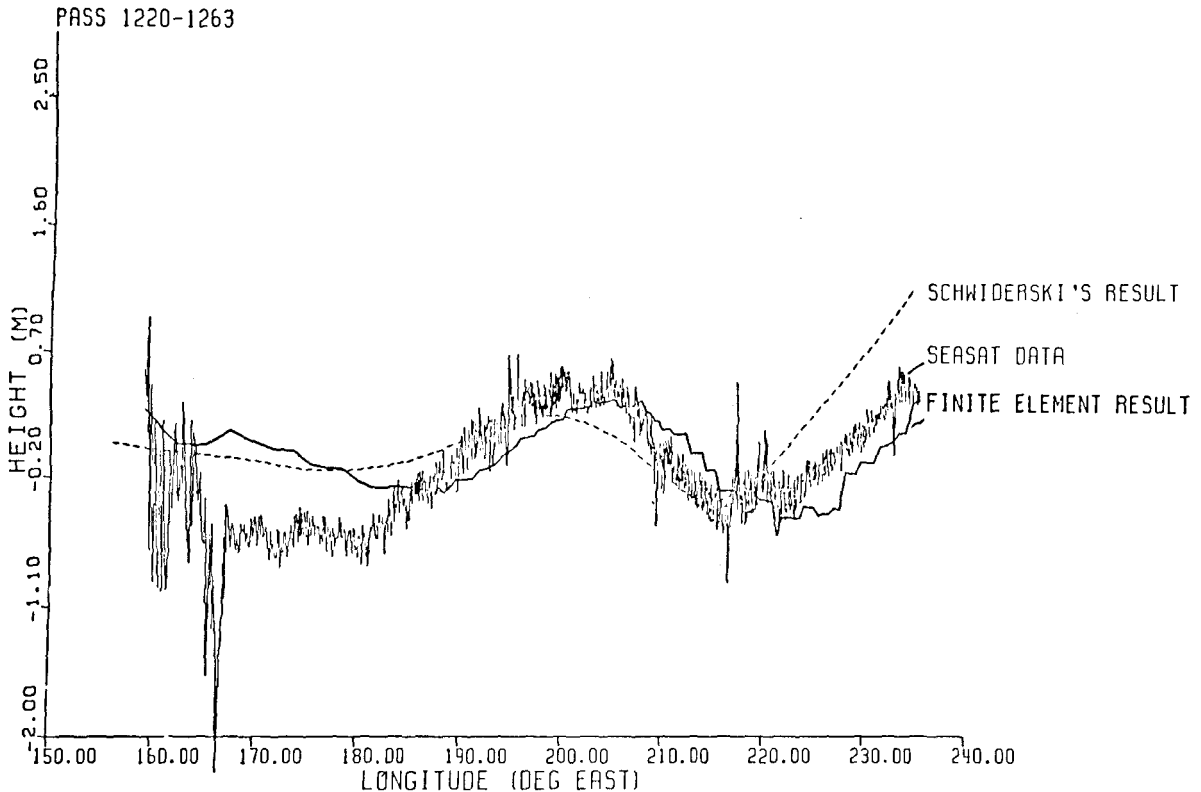


*Fig. 16a: Comparisons of the SEASAT altimeter data, Schwiderski's tidal model with our finite-element tidal model in the Pacific Ocean for passes 1220–1263.*

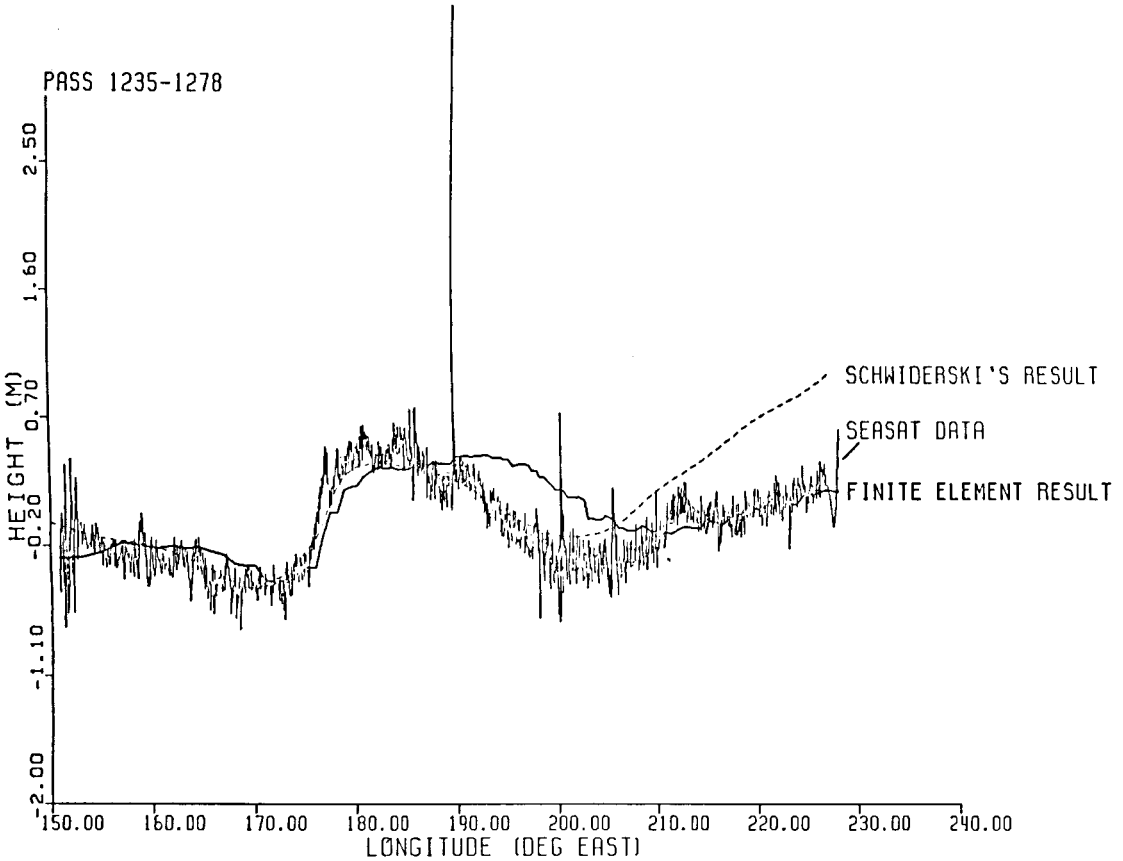


*Fig. 16b: Comparisons of the SEASAT altimeter data, Schwiderski's tidal model with our finite-element tidal model in the Pacific Ocean for passes 1235–1278.*

1235 and 1278, respectively. The Schwiderski's model contains nine harmonic partial tides of semi-diurnal ($M2, S2, N2, K2$), diurnal ($K1, O1, P1, Q1$) and long-period (mf) species. Our finite-element global tidal model represents the total tide astronomically driven by the tidal generating forces of the Moon to the second and third order of the Legendre polynomial, and of the Sun to the second order of the Legendre polynomial. Both the tidal models take into account the influence of the tidal and load deformations of an elastic Earth, according to Pekeris (1978).

For passes 1220 and 1263,

(a) our finite-element tidal model (FETM) fits the SEASAT data (SSD) better than the Schwiderski's tidal model (STM) over the northeastern Pacific Ocean and Gulf of Alaska, where there are no tide-gauge observations available,
(b) there is a phase difference between FETM and STM, and a phase difference between the two tidal models and SSD in the region of 180°−220° E. Long., and
(c) both the tidal models do not fit SSD well in the region of 160°−190° E. Long. with a difference of about 0.6 m.

For passes 1235 and 1278,

(a) except it suffers a maximum difference of about 0.8 m in comparison with SSD in the northeastern Pacific Ocean and Gulf of Alaska, STM fits SSD nearly perfectly between 150°−195° E. Long., and
(b) except there is a maximum difference of about 0.45 m between FETM and SSD in the region of 190°−210° E. Long., FETM fits SSD virtually perfectly (Kuo and Chu, in preparation).

## Conclusions

The success of Schwiderski's tidal model is based on his use of tide-gauge observations to constrain Zahel's tidal model, which was based on solving the Laplace's Tide Equations by means of the finite difference method.

It is now evident that the problem of the tides and currents of the global oceans can be profitably modeled by solving the vertically integrated hydrodynamic (or shallow-water) equations by means of the semi-implicit finite-element method, without resorting to any tide-gauge observational constraints, as we have done. We have used the SEASAT altimeter data to compare Schwiderski's tidal model results with our finite-element tidal model results. As a test, we chose the Pacific Ocean, where the tide-gauge observations are lacking particularly in the regions of the northeastern Pacific Ocean and Gulf of Alaska. We found that

1. Schwiderski's tidal model deteriorates in the region, where tide-gauge observations are lacking, and
2. our finite-element tidal model preserves its integrity and achieves a uniform precision and reliability throughout the ocean.

One of the principal advantages of our finite-element tidal model lies in the fact that it

does not rely on any tide-gauge observational constraints, and fundamentally solves the equations of motion for the said problem.

## Acknowledgements

The research was supported by the Office of Naval Research under Contract N00014-82-K-0782. The author is indebted to Mr. John G. Heacock for his encouragement.

The author is grateful to the Alexander von Humboldt Stiftung of the Federal Republic of Germany for the Humboldt Award in 1987; he expresses his special thanks to Institut für Geophysik, Technische Universität Clausthal, in particular Professor and Mrs. Otto Rosenbach, for their extraordinary hospitality.

The author thanks his collaborators, Drs. F. Malone, Y. H. Chu, and N. M. Chen for their contributions to the Tide Project at Columbia University.

Professor W. Zahel, Institut für Meereskunde der Universität Hamburg, kindly reviewed the manuscript.

## References

Bjerkness, V., Bjerkness, J., Solberg, H. and Bergeron, T. (1933): Physikalische Hydrodynamik, Springer.

Choy, L. W. and Grunes, M. R. (1986): Comparison of Ocean Tide Models with Satellite Altimeter Data, Naval Research Laboratory (NRL), Memorandum Report 5866.

Dietrich, G. (1944): Die Schwingungssysteme der halb- und eintägigen Tiden in den Ozeanen, Veröffentl. Inst. Meereskunde, Univ. Berlin, A 41, 1–68.

Hendershott, M. C. and Munk, W. H. (1970): Tides, Ann. Rev. Fluid Mech., 2, 205–224.

Kuo, J. T., Chen, N. M. and Chu, Y. H. (1986a): Time-domain Total Tides and Currents of North Atlantic Ocean with New York Bight Included, in Proc. Tenth Int. Symp. on Earth Tides, Madrid, Spain, 1985: ed. by R. Vieira, Consejo Superior de Investigaciones Cientificas, Madrid, Spain, 577–586.

Kuo, J. T., Chu, Y. H. and Chen, N. M. (1986b): Time-domain Finite-Element Modeling of the Global Ocean Tides, in Proc. Tenth Int. Symp. on Earth Tides, Madrid, Spain, 1985: ed. by R. Vieira, Consejo Superior de Investigaciones Cientificas, Madrid, Spain, 559–576.

Kuo, J. T. (1987): Ocean Dynamics, Final Report to the Office of Naval Research for Contract N00014-75-C-0605 and N00014-82-K-0782, Lamont-Doherty Geological Observatory and Aldridge Laboratory of Applied Geophysics, Columbia University, 202 p.

Kuo, J. T. and Chu, Y. H.: Comparison of the SEASAT Altimeter Data with Tidal Models, in preparation.

Malone, F. D. and Kuo, J. T. (1981): Semi-Implicit Finite-Element Methods Applied to the Solution of the Shallow Water Equations, J. Geophys. Res., 86, C5, 4029–4040.

Miles, J. W. (1974): On Laplace's Tidal Equations, J. Fluid Mech., 66–2, 241–260.

Parke, M. E. and Hendershott, M. C. (1980): M2, S2, K1 Models of the Global Ocean Tide of an Elastic Earth, Marine Geodesy, 3, 379.

Pekeris, C. L. and Accad, Y. (1969): Solution of Lapace's Equations for M2 Tide in the World Oceans, Phil. Trans. Roy. Soc. London, A 265, 413–436.

Pekeris, C. L. (1978): The Bodily Tide and the Buildup of the Earth due to Tidal Loading, Geophys. J. R. Astron. Soc., 52, 471–478.

Proudman, J. (1942): On Laplace's Differential Equations for the Tides, Proc. Roy. Soc., A 179, 261–288.

Schwiderski, E.W. (1980a): Ocean Tides, Part I: Global Tidal Equations, Marine Geodesy, 3, 161.

Schwiderski, E.W. (1980b): Ocean Tides, Part II: A Hydrodynamical Interpolation Model, Marine Geodesy, 3, 219.

Schwiderski, E.W. (1980c): On Charting Global Ocean Tides, Reviews of Geophysics and Space Physics, 18, 243.

Schwiderski, E.W. and Szeto, L.T. (1981): The NSWC Global Ocean Tide Data Tape (GOTD), Its Features and Application, Random-point Tide Program, NSWC TR 81–254.

Tiron, K.D. Sergeev, Y.N. and Michurin, A.N. (1967): Maps of Tides in the Pacific, Atlantic and Indian Oceans, Vest Leningrad University, 24, 123–135.

West, G.B. (1981): SEASAT Satellite Radar Altimetry Data Processing System, Naval Surface Weapons Center Technical Report NSWC TR 81–234.

Zahel, W. (1970): Die Reproduktion gezeitenbedingter Bewegungsvorgänge im Weltozean mittels des Hydrodynamisch-Numerischen Verfahrens, Mitteilungen des Instituts für Meereskunde der Universität Hamburg, Nr. XVII.

Zienkiewicz, O.C. (1977): The Finite-Element Method in Engineering Science: New York, N.Y., McGraw-Hill, 3rd ed., 787 p.